Numerical and Experimental Investigation of Coupled Heat and Moisture Transport Problems

John Grunewald, Dr.-Ing. **Rudolf Plagge, Dr.-Ing.** **Peter Häupl, Dr.-Ing.**

ABSTRACT

This paper describes a general thermodynamic model, including the constitutive equations, and applies it to the coupled heat and moisture transfer in porous building materials. The resulting balance equation system and the constitutive equations for the quantities considered can be numerically solved.

The constitutive equations describe the phase-divided moisture transport (liquid water flux and water vapor diffusion/advection) leading into phase-divided defined hygric transport coefficients of the balance equation system. Currently, it is impossible to separate liquid water flux and water vapor transport experimentally. To circumvent these difficulties, moisture conductivities and a phase-dividing function are introduced. For a known phase-dividing function, the phase-divided defined transport coefficients of the balance equation system can be calculated from the measured moisture conductivities. The paper presents a numerical investigation of a phase-dividing function evaluation and a description of laboratory experiments required for material characterization.

INTRODUCTION

The modeling of coupled heat and moisture transfer has recently been a major research topic in the field of building physics (Arfvidsson 1998; Brocken 1998; Descamps 1997; Grunewald and Houvenaghel 1998; Krus 1996; Roels 2000). This paper describes a general thermodynamic model, including the constitutive equations, and applies it to the coupled heat and moisture transfer in porous building materials. The resulting balance equation system and the constitutive equations for the quantities considered can be numerically solved.

MODELING OF COUPLED HEAT AND MOISTURE TRANSFER

Balance Equations

The general thermodynamic model, including the constitutive equations, derived in Grunewald and Houvenaghel (1998) can be applied to the coupled heat and moisture transfer in porous building materials. The phase system is considered as consisting of three phases, a solid (m), a liquid (l), and a gaseous (g) phase. General component mass balance equations are applied to the components of the gaseous phase: dry air (a) and water vapor (v). Eliminating the rates of phase change, the liquid water and the water vapor balance are added, which results in a moisture balance. Furthermore, the balance equation of internal energy is established to describe the thermal behavior of the system.

The modeling can be simplified, if the following assumptions are accepted. The gaseous phase is considered as a binary system consisting of dry air and water vapor. The partial pressures of dry air and water vapor form the gas pressure $p_g = p_a + p_v$. Gravity is the only volumetric force taken into account, and the mass production terms contain only phase changes. The production of internal energy by compression and friction is assumed to be negligible in the energy balance equation. In the macroscopic balance equations, the volumetric content of the liquid phase θ_l and of the gaseous phase θ_g are used instead of volume-integrated

John Grunewald and **Rudolf Plagge** are research scientists and **Peter Häupl** is a professor and head of the Institute of Building Climatology, Faculty of Architecture, University of Technology, Dresden, Germany.

microscopic indicator functions. For the above assumptions, the moisture mass balance and the internal energy balance read in local formulation as in Equations 1 and 2.

$$\frac{\partial}{\partial t}[\rho_l\theta_l + \rho_v\theta_g] = -\frac{\partial}{\partial x_k}[\rho_l v_k^{m_l}\theta_l + j_{k,diff}^{m_v}\theta_g] \quad (1)$$

$$\frac{\partial}{\partial t}[\rho_m u_m + \rho_l u_l\theta_l + \rho_v u_v\theta_g] = -\frac{\partial}{\partial x_k}[j_{k,diff}^{Q} + \rho_l u_l v_k^{m_l}\theta_l + h_w j_{k,diff}^{m_v}\theta_g] \quad (2)$$

The left-hand side of the balance equations (1 and 2) describes the storage of moisture and internal energy, and the terms at the right-hand side present the divergences of total flux of these quantities.

Constitutive Equations

The balance equations for the description of nonisothermal moisture transfer define three independent flux expressions. They can be formulated by constitutive equations for advective liquid water flux (Equation 3), water vapor diffusion (Equation 4), and heat flux (Equation 5).

Liquid water flux

$$\rho_l v_k^{m_l} = -K_t\frac{\partial p_c}{\partial x_k} \quad (3)$$

Water vapor diffusion

$$j_{k,diff}^{m_v} = -\rho_g D_{vn}\frac{\partial c_v}{\partial x_k} = -\frac{D_{vn}}{R_v T}\frac{\partial p_c}{\partial x_k} \quad (4)$$

Heat flux

$$j_{k,diff}^{Q} = -\lambda\frac{\partial T}{\partial x_k} \quad (5)$$

The hygric transport coefficients K_l and D_{vn} have been introduced in a phase-divided manner, i.e., they describe liquid water flux and water vapor diffusion separately. As stated above, a phase-divided measurement of moisture flux is not possible with the current state-of-the-art moisture transport measurement technology. The determination of vapor diffusion coefficients is affected by liquid water transport, which has lead to different approaches of moisture-dependence of the vapor diffusivity in the past (Krischer 1942; Neiß 1982; Kießl 1983; Häupl and Stopp 1987). On the other hand, the determination of the liquid water conductivity in the unsaturated moisture range is not possible without being influenced by vapor transport in the gaseous phase. That means the required coefficients for numerical simulation are not directly measurable according to their definitions. This leads to the conclusion that the phase-divided introduction of moisture transport coefficients in terms of primary material properties is problematic. Therefore, K_l and D_{vn} should be regarded as secondary material properties that can be calculated from the primary ones. In order to relate K_l and D_{vn} to primary properties (i.e., moisture conductivities), a phase-dividing function describing the percentages of liquid and vapor flux as part of the total moisture flux is introduced.

Introduction of a Phase-Dividing Function

The moisture flux can be written in terms of different driving forces, such as gradients of capillary pressure, vapor pressure, and temperature. These driving forces result from the governing thermodynamic potentials.

The capillary pressure is related to the relative humidity and to the vapor pressure by the Kelvin equation $p_c = \rho_l R_v T\ln(\varphi)$. The vapor pressure gradient can be expressed by the gradients of capillary pressure and temperature as shown in Equation 6.

$$\frac{\partial p_v}{\partial x_k} = \frac{\rho_v}{\rho_l}\frac{\partial p_c}{\partial x_k} + \frac{\partial p_v}{\partial T}\frac{\partial T}{\partial x_k} \quad (6)$$

Replacing the capillary pressure gradient and the vapor pressure gradient in Equations 3 and 4 by the relation in Equation 6, the alternative formulations, Equations 7 and 8, are obtained for both the liquid and gaseous water flux.

$$\rho_l v_k^{m_l} = -\left[K_l\frac{\rho_l}{\rho_v}\right]\frac{\partial p_v}{\partial x_k} + \left[K_l\frac{\rho_l}{\rho_v}\frac{\partial p_v}{\partial T}\right]\frac{\partial T}{\partial x_k} \quad (7)$$

$$j_{k,diff}^{m_v} = -\left[\frac{D_{vn}}{R_v T}\frac{\rho_v}{\rho_l}\right]\frac{\partial p_c}{\partial x_k} + \left[\frac{D_{vn}}{R_v T}\frac{\partial p_v}{\partial T}\right]\frac{\partial T}{\partial x_k} \quad (8)$$

The total moisture flux is the sum of the volumetric content-weighed mass fluxes of liquid and gaseous water,

$$j_k^{m_w} = \rho_l v_k^{m_l}\theta_l + j_{k,diff}^{m_v}\theta_g\,.$$

The addition of the expressions in Equations 3, 4, 7, and 8, containing the same driving forces, yields the total moisture flux (Equation 9).

$$j_k^{m_w} = K_c\frac{\partial p_c}{\partial x_k} - \left[\frac{D_{vn}}{R_v T}\frac{\partial p_v}{\partial T}\theta_g\right]\frac{\partial T}{\partial x_k} = -K_h\frac{\partial p_v}{\partial x_k} + \left[K_l\frac{\rho_l}{\rho_v}\frac{\partial p_v}{\partial T}\theta_t\right]\frac{\partial T}{\partial x_k} \quad (9)$$

Capillary moisture conductivity

$$K_c(\theta_l, T) = \underbrace{K_l\theta_l}_{f_{lg}K_c} + \underbrace{\frac{D_{vn}}{R_v T}\frac{\rho_v}{\rho_l}\theta_g}_{(1-f_{lg})K_c} \quad (10)$$

Hygroscopic moisture conductivity

$$K_h(\theta_l, T) = \underbrace{K_l \frac{\rho_l}{\rho_v}\theta_l}_{f_{lg}K_h} + \underbrace{\frac{D_{vn}}{R_v T}\theta_g}_{(1-f_{lg})K_h} \tag{11}$$

From Equation 9, it can be said that the moisture movement through a porous medium under nonisothermal conditions is caused by the gradients of capillary pressure (or vapor pressure) and temperature. According to the driving forces, moisture conductivities can be introduced. These are the capillary moisture conductivity K_c, due to the capillary pressure gradient, and the hygroscopic moisture conductivity K_h, due to the vapor pressure gradient.

The moisture flux under isothermal conditions can be alternatively described by the hygroscopic moisture conductivity K_h in the hygroscopic moisture range and the capillary moisture conductivity K_c in the overhygroscopic moisture range.

$$(j_k^{m_w})_T = \begin{cases} -K_h(\theta_l, T)\dfrac{\partial p_v}{\partial T} & 0 \le \theta_l \le \theta_{Hyg} \\ -K_c(\theta_l, T)\dfrac{\partial p_c}{\partial T} & \theta_{Hyg} < \theta_l \le \theta_{Sat} \end{cases} \tag{12}$$

The above definition of a phase-dividing function $f_{lg}(\theta_l, T)$, as shown in Equations 10 and 11, allows one to calculate K_l and D_{vn} from the moisture conductivities K_c and K_h, as shown in Equations 13 and 14.

$$K_l\theta_l = f_{lg}(\theta_l, T)\, K_c(\theta_l, T) \tag{13}$$

$$D_{vn}\theta_g = [1 - f_{lg}(\theta_l, T)]\, K_h(\theta_l, T)\, R_v T \tag{14}$$

The moisture conductivities must be experimentally determined, preferably as function of moisture content and temperature.

Saturated moisture conductivity

$$K_c(\theta_{Sat}, T) = K_{Sat}(T)$$

Relative hygroscopic moisture conductivity

$$\frac{K_h(\theta_l, T)}{K_{Sat}(T)} = K_{h,r}(\theta_l) \qquad (0 \le \theta_l \le \theta_{Hyg})$$

Relative capillary moisture conductivity

$$\frac{K_c(\theta_l, T)}{K_{Sat}(T)} = K_{c,r}(\theta_l) \qquad (\theta_{Hyg} < \theta_l \le \theta_{Sat})$$

The remaining task is the determination of the phase-dividing function $f_{lg}(\theta_l, T)$. A concept for experimental determination of the phase-dividing function under steady-state conditions is presented below.

Numerical Solution

The modeling of transient transport processes leads into a system of nonlinear differential equations that can be solved by numerical integration in time. The variables of state (moisture contents, temperatures, diffusive and advective fluxes of liquid water, water vapor, heat, etc.) can be obtained by dependence on space and time.

In order to support the investigation of the coupled heat, air, salt, and moisture transport in porous building materials, the numerical simulation program DELPHIN4 (formerly DIM3.1, Grunewald 2000a and 2000b) has been developed. The simulation of the hygrothermal transport processes in porous materials is possible for one-dimensional, two-dimensional, and axial-symmetric three-dimensional problems. The program can be used in order to simulate transient mass and energy transport processes under arbitrary climatic boundary conditions (temperature, relative humidity, driving rain, wind speed, wind direction, short- and long-wave radiation). Additionally, laminar air flux and salt diffusion/convection processes can be simulated with DELPHIN4. The investigation of the influence of salt contamination on hygric transport properties is currently a topic of research.

Determination of the Phase-Dividing Function

It could be shown by numerical investigations (Grunewald 2000c) that a phase-dividing function can have an essential influence on nonisothermal moisture transport processes. Especially for drying experiments or experiments with opposite liquid water flux and vapor diffusion, the phase-dividing function determines the slope of the moisture front. A steep moisture gradient forms between the hygroscopic and the capillary areas when the vapor diffusion prevails in the liquid water flux; otherwise, a more equalized moisture distribution can be observed. Therefore, the knowledge of the moisture content profile (beside other state quantities) should enable the determination of the phase-dividing function.

In order to determine the phase-dividing function under steady-state and nonisothermal moisture transport conditions, the experimental setup shown in Figure 1 is proposed. An

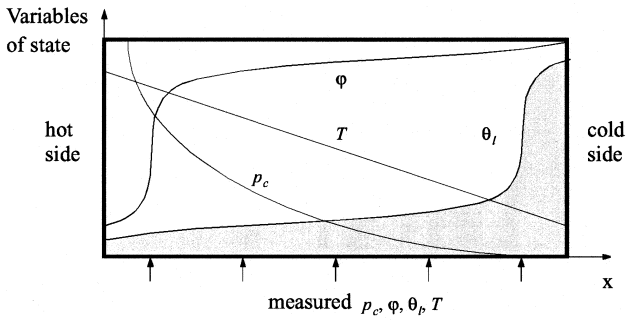

Figure 1 *Experimental conditions for determination of the phase-dividing function.*

initially moist sample is sealed at the whole surface and a temperature gradient is applied. The vapor diffusion follows the temperature gradient and leads to a liquid water accumulation at the cold side. Under steady-state conditions, the water vapor flux equals the backward liquid water flow. The profiles of capillary pressure, relative humidity, moisture content, and temperature have to be measured (at different positions and in time because it has to be controlled whether or not steady-state conditions are reached). As shown in the following derivation, the steady-state profiles give the information about a "steady-state" phase-dividing function.

For the above assumptions, the total moisture flux (Equation 9) is zero and reduces to Equation 15. Because of the steady-state conditions, the variables depend only on the position, not on time. Therefore, the gradients may be written as total derivatives instead of partial derivatives.

$$\begin{aligned} j_k^{m_w} &= -K_c\frac{\partial p_c}{\partial x_k} - \left[\frac{D_{vn}}{R_v T}\frac{\partial p_v}{\partial T}\theta_g\right]\frac{\partial T}{\partial x_k} = 0 \qquad 0 \le \theta_l \le \theta_{Hyg} \\ j_k^{m_w} &= -K_h\frac{\partial p_v}{\partial x_k} + \left[K_l\frac{\rho_l}{\rho_v}\frac{\partial p_v}{\partial T}\theta_t\right]\frac{\partial T}{\partial x_k} = 0 \qquad \theta_{Hyg} < \theta_l \le \theta_{Sat} \end{aligned} \tag{15}$$

Using the definitions of the capillary and the hygroscopic moisture conductivity, the transport coefficients can be eliminated and Equation 15 is rewritten as Equation 16. It can be denoted as hygroscopic and capillary reduced formulation of the phase-dividing function.

$$\begin{aligned} \frac{dp_v}{dx_k} + f_{lg}\left[\frac{\partial p_v}{\partial T}\right]\frac{dT}{dx_k} &= 0 \qquad 0 \le \theta_l \le \theta_{Hyg} \\ \frac{dp_c}{dx_k} + (1 - f_{lg})\left[\frac{\rho_l}{\rho_v}\frac{\partial p_v}{\partial T}\right]\frac{dT}{dx_k} &= 0 \qquad \theta_{Hyg} < \theta_l \le \theta_{Sat} \end{aligned} \tag{16}$$

Using the Kelvin equation as

$$p_v = p_{vs}\varphi = p_{vs}\exp\left(\frac{p_c}{\rho_l R_v T}\right), \tag{17}$$

the partial temperature derivation of the water vapor pressure is

$$\left[\frac{\partial p_v}{\partial T}\right] = \varphi\frac{\partial p_{vs}}{\partial T} + p_{vs}\frac{\partial \varphi}{\partial T}, \tag{18}$$

and the product of the density ratio and the temperature derivation of the vapor pressure reduces to

$$\left[\frac{\rho_l}{\rho_v}\frac{\partial p_v}{\partial T}\right] = \frac{\rho_l R_v T}{p_{vs}}\frac{\partial p_{vs}}{\partial T} + \frac{\partial p_c}{\partial T} - \frac{p_c}{T}. \tag{19}$$

With Equations 18 and 19, the reduced formulations in Equation 16 are used to express the moisture and temperature dependence of the phase-dividing function as shown in Equation 20.

$$\begin{aligned} f_{lg}(\theta_l, T) &= \frac{1}{\varphi\dfrac{\partial p_{vs}}{\partial T} + p_{vs}\dfrac{\partial \varphi}{\partial T}}\frac{dp_v}{dT} \qquad 0 \le \theta_l \le \theta_{Hyg} \\ f_{lg}(\theta_l, T) &= 1 + \frac{1}{\dfrac{\rho_l R_v T}{p_{vs}}\dfrac{\partial p_{vs}}{\partial T} + \dfrac{\partial p_c}{\partial T} - \dfrac{p_c}{T}}\frac{dp_c}{dT} \qquad \theta_{Hyg} < \theta_l \le \theta_{Sat} \end{aligned} \tag{20}$$

The functions dp_v/dT and dp_c/dT can be directly determined from the above described experiment by measurement of the capillary pressures (in the hygroscopic range, the vapor pressures) and the temperatures. If the moisture retention curve is regarded as a function of capillary pressure, relative humidity, and temperature, $\theta_l = \theta_l(p_c, T)$ and $\theta_l = \theta_l(\varphi, T)$, then the dependence of the reverse moisture retention functions on the temperature, $\partial p_c/\partial T$ and $\partial\varphi/\partial T$, have to be known for this experiment.

Because the phase-dividing function can be directly calculated from state variables, it should be possible to reproduce an initial guess of the phase-dividing function (input for numerical simulation) for the above described experiment. A numerical investigation has been carried out for the above problem and Equation 20 was confirmed, i.e., the phase-dividing function used on input could be reproduced from the numerical results of capillary pressure, relative humidity, moisture content, and temperature.

Figure 2 shows an evaluation of the numerical output of the DELPHIN4 program using Equation 20. The investigation was done for different initial moisture contents (indicated by lines 1-9) and for both the hygroscopic (hyg) and capillary (cap) formulation of Equation 20. The longest line represents the DELPHIN4 input curve. Lower initial moisture contents allow the reproduction of the lower parts of the phase-dividing function. The higher the initial moisture contents, the smaller the range of the curve obtained. Additionally, the numerical simulation of such an experimental setup allows the investigation of the influence of errors, such as the shortening of the measuring time (i.e., non-steady-state conditions).

DETERMINATION OF HYGRIC MATERIAL PROPERTIES

Equipment

In order to evaluate numerical transport models describing the hygric behavior of capillary porous materials, it was deemed necessary to develop an experimental setup designed to accurately and rapidly determine hydraulic properties of capillary porous media. The laboratory methods should be able to measure the moisture storage and transport simultaneously.

To achieve this objective, a sophisticated instantaneous profile method was developed. A standard material container can be equipped by different types of sensors to investigate the flow process within the material sample. The development of time domain reflectometry (TDR) as a new technique to deter-

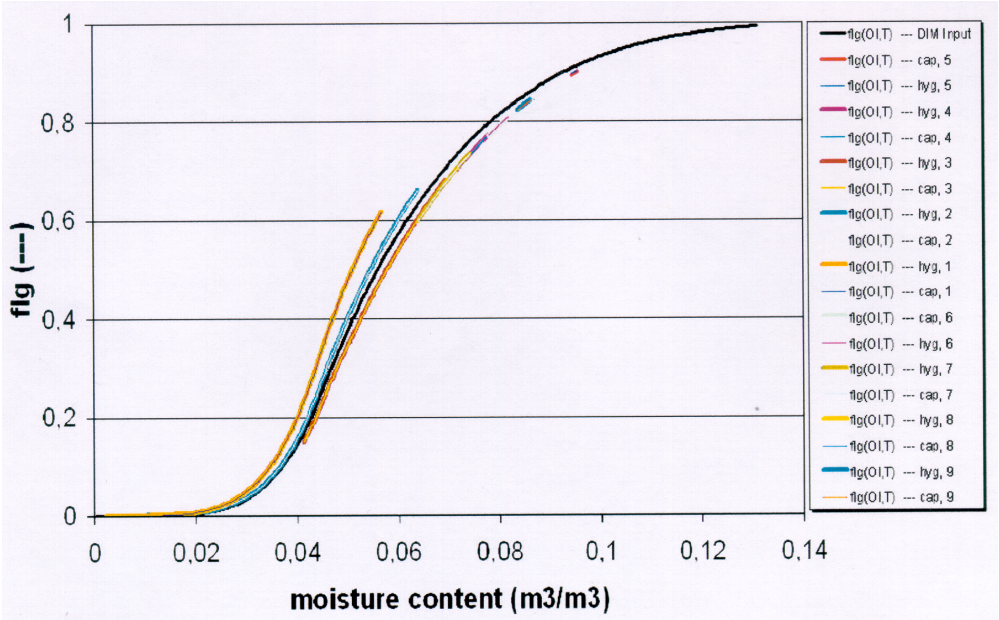

Figure 2 *Evaluation of numerical simulation results with an initial guess of the phase-dividing function.*

mine water content opened possibilities for an accurate, non-destructive laboratory method to determine water content in a high temporal and spatial resolution. Therefore, we undertook a major effort to incorporate the TDR technique with miniaturized probes (Malicki et al. 1992) as a basic tool in the method. Miniaturized pressure transducer tensiometers (Plagge 1991) and relative humidity sensors are used for the determination of the water potential in the wet and dry moisture range. The basic idea for the development of the method is the use of a same material column in a series of experiments, where different flow regimes can be achieved by controlling the initial and boundary conditions.

In general, the experimental setup consists of several components. The vertical measuring sampler is provided with five pairs of trapped holes, into which guide nuts are screwed prior to drill holes and specially designed sensors are inserted. The material sample is equipped by TDR-unimpressible and pressure transducer tensiometers or relative humidity sensors, aligned at equal distances of 20 mm along the 100-mm-long container. Movement of water can be achieved by controlling the evaporation, where a ventilator is used to control the evaporation rate and to realize constant relative humidity boundary condition. A lid with sealing material serves for zero flux boundary conditions at the bottom (IPM I) and the top (IPM II) of the material sample. To monitor, control, and register material moisture and water potential, a computer-aided automatic data acquisition system is used. Further information concerning the sensors used, their calibration, and additional experimental details are given by Malicki et al. (1992), Plagge et al. (1996, 1997, 1990), and Plagge (1991).

Experiments

For measurement, the material is sampled, pre-wetted, fixed into a standard container, and prepared for sensor installation. The material sample is equipped by mini-tensiometers and TDR probes and sealed at the bottom. At the top of the sample, a ceramic plate is fixed and a controlled suction of –10 hPa is applied. Static equilibrium was achieved after several days, indicated by time-constant water content and water potential in different positions measured by the TDR and the tensiometer system.

IPM I. To start the experiment, the ceramic plate is removed and the ventilator and/or lids with holes are placed on the top of the sample. Thus, the material is allowed to evaporate while water content and water potential are monitored continuously. When the end of the experiment is reached, the water content measured by the top TDR sensor is equal to the one measured at 95% relative humidity. Subsequently, the tensiometers are removed and the material container is placed into a climatic chamber for equilibration at a relative humidity of 95%.

IPM II. To start the second experiment, the relative humidity sensors are installed into the sample container. The top of the sample is sealed and the sampling container is fixed on the miniaturized climatic chamber box, where a ventilator is used to control the relative humidity and dry the material. During the desorption, water content and relative humidity are continuously monitored and registered by the acquisition system.

After the experimental runs, the different sensors are removed and the total water content of the sample is measured by thermo-gravimetry. From measurement of the sample mass

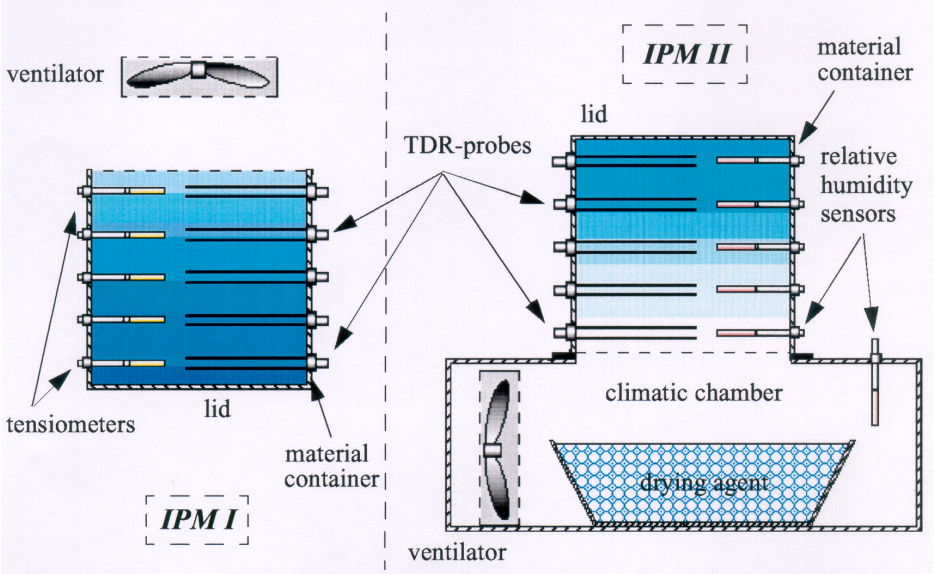

Figure 3 *Schematic view of the two instantaneous profile methods, IPM I and IPM II, used for the simultaneous determination of the desorption characteristics of the storage and transport of the material moisture.*

at the beginning of each IPM run, the TDR water content measurements are corrected using a mixed dielectric component approach (Plagge et al. 1996). An adjustment of the tensiometers and the relative humidity sensors is done by defining a physical offset at the static equilibrium before each IPM run.

Calculations

As a result of the experiments, three different measurement ranges can be distinguished. The first tensiometer range is from saturation up to 1 bar capillary pressure, the second range is from 1 bar up to 60 bar capillary pressure, and the relative humidity range is <95%, which is equivalent to >60 bar capillary pressure. Since there is no water potential sensor available in the range between 1 to 60 bar, the capillary pressure was indirectly derived from the static water retention characteristics and the corresponding water content determined by TDR. For calculation and data interpretation, each range is interpreted individually.

During the experimental runs, water content and capillary pressure (water potential) are measured (derived, for the second measurement range) at five different positions along the vertical material sample, resulting in two sets of data of water contents and capillary pressures. Each single measurement corresponds to a triplet (water content or capillary pressure as a function of position and time); all together design a surface in a three-dimensional coordinate. The interpolation of the triplets results in a surface of smoothed data sets. Assuming the measurement error is of pure stochastic nature, a part of the measurement error can be removed by the three-dimensional interpolation procedure according to Bezier (1971). On this basis, it is possible to generate smoothed values, given by a number of generated values based on the measured values.

The calculation of a smoothed water content and water potential surface is required in a rectangular coordinate. The length of the steps can be calculated in arbitrary density. As a result of the smoothing procedure, one yields the surfaces of the measurement variables for a given position at a defined time. From the corresponding water content and water potential time-profiles, the storage characteristics for chosen compartments of the material can be determined. The smoothing procedure described above is not only used to interpolate the data collected at different measurement times. One can imagine that each single set of data corresponds to a defined mass. The bigger the data density, the larger their mass and the more strongly the smoothed and new constructed surface is attracted. Thus, the stochastic errors can be removed by the procedure. By contrast, if systematic biased errors occur, e.g., a sensor drift induced by temperature or a wrong offset, this would lead to a continuous shift of measurement data and would be reflected by the smoothing procedure. On the other hand, real effects, shown by continuously higher or smaller values, are not masked by the interpolation procedure.

Results and Discussion

As an example, results are shown for calcium silicate panels, a material that is used for inside insulation. Figure 4 presents the water retention characteristics measured by the transient IPM methods. For comparison, the data from standardized thermo-gravimetric reference methods are also shown in the plot. The reference data were measured in six replicates by the pressure plate apparatus (ISO 1993) and desiccators with different saturated salt-in-water solutions (ISO 1996). These results correspond to static equilibrium conditions. While the IPM applications needed less than one month to scan all of the characteristics simultaneously, the

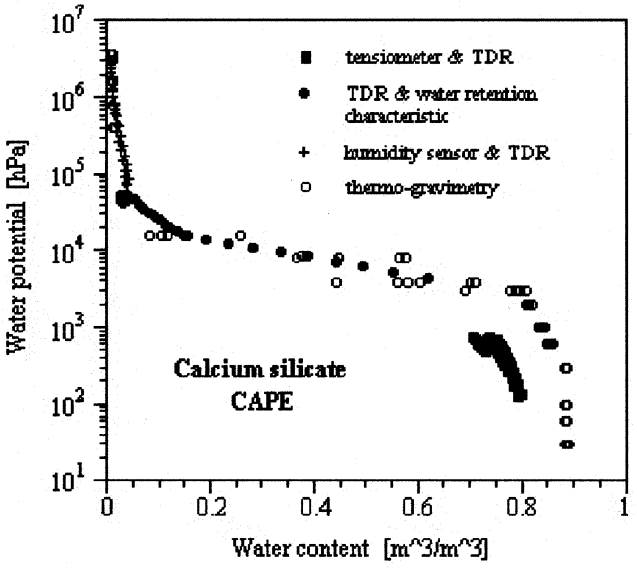

Figure 4 *Comparison of the IPM methods and classical static equilibrium methods to determine the water retention characteristics of the calcium silicate panels. The variables* θ_{Sat} *and* Φ *correspond to the saturated water content after capillary saturation and the porosity after vacuum saturation.*

static equilibrium methods required a time of more than one year.

The water retention data represent the complete storage characteristics of the calcium silicate material. In the dry and wet moisture range, the static state data show a small variation within their replicates. Starting at a water potential of 300 hPa, which represents the air-entry-point of the material, the results indicate an increasing scatter within the replicates. The maximum difference is reached at 3000 hPa (about 3 bar capillary pressure), where the scatter exceeds a volumetric moisture of about $\theta = 0.25\ m^3/m^3$. These variations within the independent replicates can be explained by the natural heterogeneity of the material.

Figure 4 indicates differences between the transient data measured by TDR and tensiometers and the static thermogravimetric reference. The reason is given by the different procedures used to saturate the samples. To receive the pore size distribution of the material by the static equilibrium methods, the material samples have been moistened using vacuum saturation. Thus, a maximum water content was achieved at $\theta = 0.90\ m^3/m^3$, corresponding to the porosity Φ of the material. For the transient methods, capillary saturation is preferably applied. At natural conditions, the pores are moistened by capillary forces only, where not all pores are water filled. As a consequence, the effective saturated water content does not exceed $\theta_{sat} = 0.81\text{-}0.84\ m^3/m^3$. A part of the variation within the IPM I data is due to spatial heterogeneity. Furthermore, transient curves depend on the speed of the imposed water content change and the initial water content, where more water is retained at a given water potential with decreasing water content and increasing capillary pressure (Plagge et al., in press).

Since the capillary potential cannot be measured within the water potential range of 10^3 to 6×10^4 hPa, the capillary pressure for the IPM method is derived from the mean static equilibrium data, thus removing any information about the variability. The transformation of this mean characteristic to the TDR data measured at the five compartments generates new scattered water potential data. This artificial scatter is removed by decreasing the spatial resolution of the Bezier (1971) fitting procedure. The smoothing character of the results is visible in the plot.

The comparison between the IPM II data and the hygric sorption isotherm as the static reference method shows close agreement. Only the enlargement of this dry range indicates that a unique relationship between water content and capillary potential does not exist. This can be explained by the spatial variability of the material and the affected transient conditions (Plagge et al., in press). The results corroborate experiments from several researchers who have found a multiplicity of curves in dynamic experiments. Since an equilibrium status over a long time interval does not exist under natural conditions, the validity of static equilibrium methods is limited.

The moisture transport characteristics as a function of the water potential and water content are shown in Figure 5. The unsaturated hydraulic conductivity is given over the whole water potential and moisture range and varies about nine orders of magnitude. The connection between the measurement ranges identifies a good collaboration between the different instantaneous profile methods.

The hydraulic conductivity in the dry and wet range is determined for five compartments along the vertical material sample. To minimize errors due to sensor drifts and biased water potential measurements, a threshold gradient is introduced, where the magnitude of the threshold depends on the accuracy of the water potential measurement. If a hydraulic gradient remained below the threshold gradient, the resultant conductivity is rejected from the data. Since the pressure transducer tensiometers exhibit a higher accuracy than the relative humidity sensors, smaller gradients are discarded from further evaluation of conductivity. This is visualized by the denseness of the data in the moist range, where five compartments can be plotted. The variations within the data are due to different initial moisture contents caused by spatial heterogeneity. No variability is shown in the water potential range between 10^3 to 6×10^4 hPa, where any scatter is removed by the decrease of the spatial resolution of ζ during the Bezier fitting procedure.

CONCLUSIONS

In general, the determination of water vapor diffusion and liquid water transport coefficients is realized by experimental methods that do not allow a distinction between the different

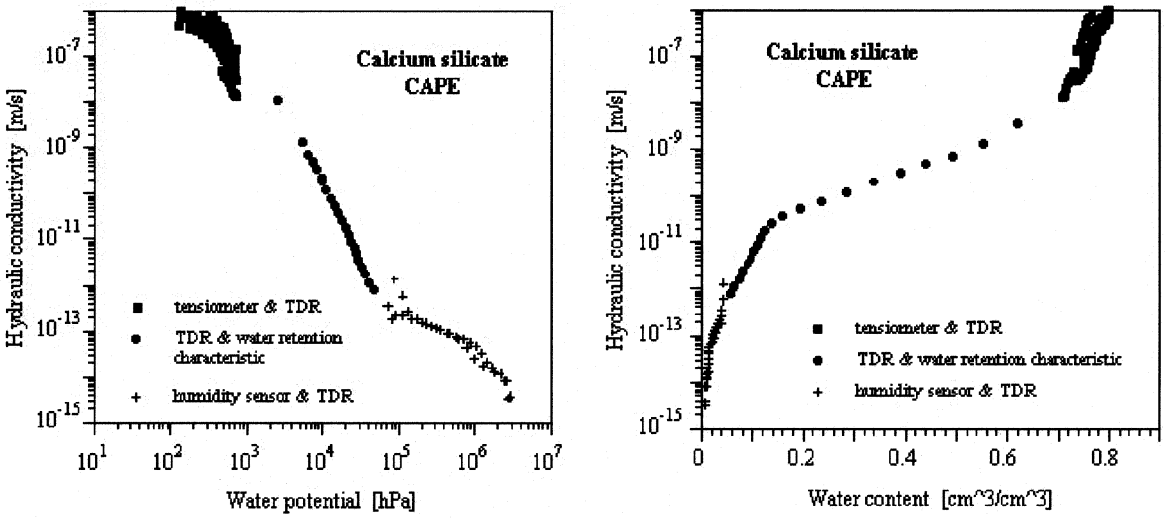

Figure 5 *Unsaturated hydraulic conductivity by the IPM methods as a function of capillary pressure (left) and water content (right) of the calcium silicate insulation panels. The capillary pressures of the data, indicated by the dots, were indirectly derived using the static water retention characteristic.*

phase states of water. Thus, a phase-dividing function can be introduced and should be determined by nonisothermal moisture and energy transport experiments. The use of transport coefficients for water vapor diffusion and liquid water transfer for computer simulations of nonisothermal problems without an experimentally determined phase-dividing function is critical and can lead to unreasonable results. A "false" phase-dividing function would lead to incorrect nonisothermal moisture transport calculations due to its influence on the water vapor diffusion according to the temperature gradient.

In a series of experiments where different nonstationary flow regimes are achieved by controlling the initial and boundary conditions, a standard material container can be equipped by a set of accurate and miniaturized nondestructive TDR sensors, pressure transducer tensiometers, and relative humidity sensors. Thus, water content and capillary water potential can be measured simultaneously in high temporal and spatial resolution during the transient experiments. For the calculation of data, a smoothing procedure (Bezier 1971) is applied to remove stochastic errors from the data.

The instantaneous profile methods presented are able to measure the water retention characteristic and the capillary moisture conductivity simultaneously in a reasonably short time. For calcium silicate insulation panels, the required measurement time was only about four weeks, while the determination of the water retention characteristics by static equilibrium reference methods needed more than one year. Disadvantageous are the demands of special sensor installation technologies and the lack of missing water potential sensors in the range between 10^3 to 6×10^4 hPa. The measurement technology should be further developed in order to determine the phase-dividing function experimentally.

NOMENCLATURE

c_m = specific heat capacity, dry material, J/kgK
c_v = mass concentration of water vapor, kg/kg
D_{vn} = vapor diffusion coefficient, m^2/s
f_{lg} = phase-dividing function
g_k, g = gravity acceleration, m/s^2
h_v = specific enthalpy of water vapor, J/kg
$j_k^{m_w}$ = total moisture flux, kg/m^2s
$j_{k,diff}^{m_v}$ = vapor diffusion flux, kg/m^2s
$j_{k,diff}^{Q}$ = heat flux, W/m^2
K_l = liquid water conductivity, s
K_c = capillary moisture conductivity, s
K_h = hygroscopic moisture conductivity, s
$K_{c,r}$ = relative capillary moisture conductivity
$K_{h,r}$ = relative hygroscopic moisture conductivity
K_{Sat} = capillary moisture conductivity at saturation, s
p_c = capillary pressure, Pa
p_g = pressure of the gaseous phase, Pa
p_v = partial vapor pressure, Pa
p_{vs} = saturation vapor pressure, Pa
p_a = partial air pressure, Pa
R_v = specific gas constant of vapor, J/kgK
T = temperature, K
t = time, s
u_m = specific internal energy of solid material, J/kg

u_l = specific internal energy of liquid phase, J/kg

u_v = specific internal energy of vapor, J/kg

$v_k^{m_l}$ = velocity of the liquid phase, m/s

x_k = spatial vector, m

Symbols

θ_l = volumetric content of liquid water, m^3/m^3

θ_g = volumetric content of the gaseous phase, m^3/m^3

θ_{Hyg} = maximum hygroscopic moisture content, m^3/m^3

θ_{Sat} = saturation moisture content, m^3/m^3

λ = thermal conductivity, W/mK

ρ_m = mass density of the solid material, kg/m^3

ρ_l = mass density of the liquid phase, kg/m^3

ρ_v = mass density of water vapor, kg/m^3

Φ = porosity, m^3/m^3

φ = relative humidity

REFERENCES

Arfvidsson, J. 1998. Moisture transport in porous media. Ph.D. thesis, Lund University.

Bear, J., and Y. Bachmat. 1992. *Introduction to modeling of transport phenomena in porous media*. Kluwer Academic Publishers.

Brocken, H.J.P. 1998. Moisture transport in brick masonry: the grey area between bricks. Ph.D. thesis, Technical University of Eindhoven.

Bezier, P.E. 1971. Example of an existing system in the motor industry: The unisurf system. *Proc. Roy. Soc.*, London A(321): 207-218.

Descamps, F. 1997. Continuum and discrete modeling of isothermal water and air transfer in porous media. Ph.D. thesis, Catholic University Leuven, Belgium.

Grunewald, J. 1997. Konvektiver und diffusiver Stoff- und Energietransport in kapillarporösen Baustoffen. Dissertation an der TU Dresden, Fakultät Bauingenieurwesen.

Grunewald, J., and G. Houvenaghel. 1998. European Project BE96-3290, *Development of a new methodology to analyse the durability of facade repair and retrofitting systems*. Final report of Task 2: Modelling.

Grunewald, J. 1999. European Project BE96-3290, *Development of a new methodology to analyse the durability of facade repair and retrofitting systems*. Final report of Task 5: Numerical simulation and program development.

Grunewald, J. 2000a. Documentation of the numerical simulation program DIM3.1. *Volume 1: Theoretical fundamentals*. DELPHIN4.1 program installation available on the ftp-server of the Institute of Building Climatology: ftp://141.30.41.194.

Grunewald, J. 2000b. Documentation of the numerical simulation program DIM3.1. *Volume 2: User's guide*. DELPHIN4.1 program installation available on the ftp-server of the Institute of Building Climatology: ftp://141.30.41.194.

Grunewald, J. 2000c. Non-isothermal transport calculations with DIM3.1. Int. Zeitschrift für Bauinstandsetzen und Denkmalpflege, 6. Jahrgang, Aedificatio Publishers, Heft 4, pp. 367-383.

Häupl P., Stopp H. 1987. Feuchtetransport in Baustoffen und Bauwerksteilen. Dissertation B, TU Dresden.

Hens, H. 1996. Heat, air and moisture transfer in insulated envelope parts. Final report of IEA-Annex 24. Leuven Lab. of Building Physics (ISBN 90-75741-02-2).

Hillel, D. 1980. *Fundamentals of soil physics*. New York: Academic Press, pp. 212-214.

ISO. 1993. *Soil quality—Determination of water retention characteristics*; *Laboratory methods.* International Standard, ISO/DIS 11 274.

ISO. 1996. *Building materials—Determination of water absorption coefficient*. European Standard, ISO/DIS 15 148.

Kirkham, D., and W.L. Powers. 1972. *Advanced soil physics*. New York: Wiley.

Jischa, M. 1982. *Konvektiver Impuls-, Wärme- und Stoffaustausch.* Vieweg Braunschweig.

Kießl, K. 1983. Kapillarer und dampfförmiger Feuchtetransport in mehrschichtigen Bauteilen – Rechnerische Erfassung und bauphysikalische Anwendung. Dissertation, Universität-Gesamthochschule Essen.

Klute, A., and C. Dirksen. *Hydraulic conductivity and diffusivity laboratory methods*. In: Klute, A. (ed.), Methods of soil analysis. Part I: Physical and mineralogical methods. 2d ed., no.9, Agronomy Series. Madison: Am. Soc. Agron. and Soil Sci. Soc. Am., pp. 687-734.

Krischer, O. 1942. Der Wärme- und Stoffaustausch im Trocknungsgut. VDI-Forschungsheft, 415: 1- 22.

Krus, M. 1996. Moisture transport and storage coefficients of porous mineral building materials. Ph.D. thesis, Fraunhofer Inst. for Building Physics.

Malicki, M.A., R. Plagge, M. Renger, and R.T. Walczak. 1992. Application of time-domain reflectometry (TDR) soil moisture miniprobe for the determination of unsaturated soil water characteristics from undisturbed soil cores. *Irrigation Sci.* 13: 65-72.

Meixner, J., and H.G. Reik. 1959. Thermodynamik der irreversiblen Prozesse. *Handbuch der Physik*, Band III/2, Springer Berlin.

Neiß, J. 1982. Numerische Simulation des Wärme- und Feuchtetransports und der Eisbildung in Böden. Fortschritt-Berichte der VDI-Zeitschriften, Reihe 3, Nr. 73, VDI-Verlag.

Pel, L. 1995. Moisture transport in porous building materials. Ph. D. thesis, Technical University of Eindhoven.

Plagge, R. 1991. Bestimmung der ungesättigten hydraulischen Leitfähigkeit im Boden. Diss. Bodenökologie und Bodengenese, Heft 3, pp. 151.

Plagge, R., C.H. Roth, and M. Renger. 1995. *Eine Labormethode und ein Berechnungsverfahren zur schnellen Ermittlung der Hysteresis von hydrophysikalischen Eigenschaften poröser Medien unter instationären Bedingungen.* In: Feuchtetag BAM 1995 Berichtsband "Feuchtigkeit in Baustoffen und Bauteilen, Messen - Rechnen - Anwenden," pp. 254-263.

Plagge, R., C.H. Roth, and M. Renger. 1996. Dielectric soil water content determination using time-domain reflectometry (TDR). In: A. Kraszewski (ed.): *Second Workshop on Electromagnetic Wave Interaction with Water and Moist Substances at the 1996 IEEE Microwave Theory and Techniques Society International Microwave Symposium in San Francisco, CA, 17 June, 16-21*, pp. 59-62.

Plagge, R., M. Renger, and P. Häupl. Effect of transient conditions on hydraulic properties of porous media. In: van Genuchten et al. (ed.), *Proceedings of the International Workshop on Characterization and Measurement of the Hydraulic Properties of Unsaturated Porous Media, Riverside, CA* (1997), in press.

Plagge, R., M. Renger, and C.H. Roth. 1990. A new laboratory method to quickly determine the hydraulic conductivity of unsaturated soil within a wide range of textures. Z. Pflanzenernähr. Bodenk. 153: 39-45.

Rawlins, S.L., and W.H. Gardner. 1963. A test of the validity of the diffusion equation for unsaturated flow of soil water. *Soil Sci. Soc. Am. Proc.*, pp. 507-511.

Roels, S. 2000. Modeling unsaturated moisture transport in heterogeneous limestone. Ph.D. thesis, Kat. U. of Leuven.

Sobczuk, H., R. Plagge, R. Walczak, and C.H. Roth. 1992. Laboratory equipment and calculation procedures to rapidly determine the effect of hysteresis on soil hydrophysical properties under nonstationary conditions. Z. f. Pflanzenernähr. Bodenk. 155: 157-163.